Mesoporous carbon nanotube aerogel-sulfur cathodes: A strategy to achieve ultrahigh areal capacity for lithium-sulfur batteries via capillary action

Zhenhan Fang [a, 1], Yufeng Luo [a, 1], Hengcai Wu [a], Lingjia Yan [a], Fei Zhao [a], Qunqing Li [a, b], Shoushan Fan [a], Jiaping Wang [a, b, *]

[a] Department of Physics and Tsinghua-Foxconn Nanotechnology Research Center, Tsinghua University, Beijing, 100084, China
[b] Frontier Science Center for Quantum Information, Beijing, 100084, China

ARTICLE INFO

ABSTRACT

A strategy to produce sulfur (S) cathodes with ultrahigh areal capacity for lithium-sulfur (Li−S) batteries is proposed. Porous carbon nanotube (CNT) aerogel@Li_2S_8 cathodes are obtained by dropping Li_2S_8 solution into the CNT aerogels that are prepared through a freeze-drying method. The three-dimensional (3D) porous structure of the CNT aerogel provides a complete electron transport network and rapid ion transport channels. Moreover, the rich mesoporous structure has an extreme capillary action on the electrolyte. Numerical simulation shows that in a surprisingly short time (2 μs), the electrolyte can be absorbed into the mesopores by capillary action and reach a stable state, limiting the "shuttle effect" of polysulfides. Based on these unique characteristics, the CNT aerogel@Li_2S_8 cathode exhibits excellent electrochemical performance. With an extremely high areal S loading of 20 mg cm^{-2}, the cathode shows an ultrahigh areal specific capacity of 22.9 mAh cm^{-2}. For the pouch cell with an areal S loading of 10 mg cm^{-2} and a low electrolyte/sulfur (E/S) ratio of 7.8 μL mg^{-1}, the areal specific capacity reaches a high value of 10.4 mAh cm^{-2}.

© 2020 Elsevier Ltd. All rights reserved.

1. Introduction

Lithium-ion batteries (LIBs) have been widely used as power sources in portable electronic devices and other fields, and lithium-incorporated electrodes have been extensively researched in the past two decades. However, the specific capacities of the existing LIBs cannot meet the requirements of the rapidly developing industries, such as electric vehicles. Therefore, it is urgent to develop new lithium batteries with higher capacities [1−3]. Among different secondary battery systems, lithium-sulfur (Li−S) battery becomes one of the most promising battery systems because of its high theoretical specific capacity (1675 mAh g^{-1}) and specific energy (2600 Wh kg^{-1}), which is almost five times of commercial LIBs [4]. However, many challenges remain and limit further development and application of Li−S batteries. Both the active material

sulfur (S) and the discharge product lithium sulfide (Li_2S) are poor electronic conductors. Besides, due to the density difference between S and Li_2S, a considerable volume expansion (~80%) of S occurs during the charging and discharging processes. Moreover, the intermediate polysulfides are soluble in the ether-based electrolyte and migrate to the anode, causing a shuttle effect. All these shortcomings lead to the low utilization of active materials and capacity loss during cycling [4−6].

Many researchers have conducted studies to solve the problems of Li−S batteries. The modification of S composite cathodes by combining S with conductive carbon materials at the nanometer scale is one of the most widely studied methods [7,8]. There are several commonly used conductive materials, such as microporous and mesoporous carbon [9−16], carbon nanotubes (CNTs) [17−20], graphene [21,22], carbon fiber [23−26], and other carbon materials [27−31]. In general, the most significant advantage of carbon materials in cathodes is that the conductive carbon materials can enhance the electronic transmission of S/Li_2S, thereby significantly improving the utilization of active materials and obtaining higher capacity. On this basis, some carbon materials with unique

---

structures can also remedy other defects of Li–S batteries. For example, while porous carbon materials provide a complete conductive network, the rich porous structures can also accommodate the volume expansion of S. In addition, graphene materials that are oxidized or element-doped have chemical functional groups on their surfaces to adsorb intermediate polysulfides and inhibit the shuttle effect. However, the preparation methods of these carbon materials with excellent structures tend to be complicated and the material cost is high. Besides, it is worth noting that most of the high specific capacity Li–S batteries reported in the literature are obtained with a low areal S loading (<2 mg cm^{-2}) and high electrolyte/sulfur (E/S) ratio (>15 μL mg^{-1}) [32,33], hence the areal capacities of the cathodes are usually less than 2.0 mAh cm^{-2}, which is not competitive compared to that of commercial LIBs (~4 mAh cm^{-2}) [34]. Therefore, the preparation of carbon material with a simple preparation process, high electrical conductivity, porosity, and shuttle inhibition has great significance for promoting the application of Li–S batteries.

Super-aligned CNT (SACNTs) is an ideal candidate [35]. SACNTs have a larger aspect ratio (~10^4) and stronger van der Waals force compared to ordinary CNTs, and many macroscopic architectures can be easily achieved based on SACNTs, such as films [36,37], buckypapers [38], and aerogels [39–41]. Aerogels constructed from SACNTs have unique advantages for use in Li–S batteries. First, the three-dimensional (3D) conductive CNT aerogel can provide a complete conductive network that makes more active materials available, enabling increased areal S loading and specific capacity. Second, the CNT aerogel has an abundant porous structure, which adapts to the volume expansion of S and enhances the stability of the cycle. Third and the most importantly, organic solvents can easily infiltrate into the CNT aerogel and the porous structure of the aerogel has a strong capillary action on the electrolyte, confining polysulfides in the cathode by the physical adsorption of the aerogel itself and thus suppressing the shuttle effect.

Herein, CNT aerogel@Li$_2$S$_8$ cathodes with all the above mentioned advantages were successfully obtained by infiltrating Li$_2$S$_8$ solution dissolved in the electrolyte as the initial active material into the CNT aerogels that were prepared by a simple freeze-drying method. The CNT aerogel@Li$_2$S$_8$ cathodes possess three advantages compared to standard S cathodes: a continuous CNT network to facilitate high-speed electron conduction; a rich mesoporous and macroporous structure to accommodate volume change of active material and to provide sufficient ion transport channels; extreme and numerous capillary actions among mesopores to confine polysulfides dissolved in the electrolyte and suppress the shuttle effect. The CNT aerogel@Li$_2$S$_8$ cathode exhibited excellent electrochemical performances. With an extremely high areal S loading (20 mg cm^{-2}) and an ultra-low E/S ratio (7.8 μL mg^{-1}), the cathode showed an ultrahigh areal capacity of 22.9 mAh cm^{-2} at 0.1C. Larger size pouch cells based on the CNT aerogel@Li$_2$S$_8$ cathodes were prepared as well and demonstrated excellent performances. The simple preparation method of the CNT aerogel and its effective mesoporous structure to alleviate polysulfide shuttle effect reveal the significant potential of CNT aerogel as a novel electrode material in practical applications of Li–S batteries.

2. Experimental

2.1. Preparation of CNT aerogels

SACNT arrays with a height of 300 μm and a diameter of 20–30 nm were synthesized on silicon wafers by chemical vapor deposition with iron as the catalyst and acetylene as the precursor. Details of the synthesis method were described in a previous paper [35]. SACNTs exhibit hydrophobic properties. In order to achieve better dispersion, 200 mg SACNTs were ultra-sonicated in 400 ml ethanol. Due to the low freezing point (-130 °C) of ethanol, the ethanol in the dispersion was replaced with deionized water for further freeze-drying. The aqueous CNT dispersion was dried in an oven at 80 °C to 10 ml, 20 ml, and 40 ml respectively according to the required densities. Afterward, the CNT dispersion was poured into a container and underwent a freeze-drying process to obtain CNT aerogels with densities of 20, 10, and 5 mg cm^{-3}, respectively. Due to the direct sublimation of water in the dispersion during the freeze-drying process, the uniform distribution of CNTs and the continuous CNT network structure were retained, leading to a 3D CNT porous aerogel.

2.2. Preparation of Li$_2$S$_8$ solution and CNT aerogel@Li$_2$S$_8$ cathodes

A mixture of Li$_2$S (Sigma-Aldrich) and S (Alfa Aesar) at a molar ratio of 1:7 was dissolved in solvent (1 M LiTFSI in DOL/DME = 1:1 vol% with 1 wt% LiNO$_3$), and Li$_2$S$_8$ solutions with concentration of 0.25 mol L^{-1} and 0.5 mol L^{-1} were prepared, respectively. By dropping 60 μL Li$_2$S$_8$ solution (0.25 mol L^{-1}) into the CNT aerogel with a diameter of 10 mm, the mass of active S material reached 3.84 mg. The S content was 43 wt%, and the areal S loading was 5 mg cm^{-2}. By dropping 60 μL or 120 μL Li$_2$S$_8$ solution (0.5 mol L^{-1}) into the CNT aerogels corresponding to 60 wt% and 75 wt% S content, the areal S loadings were 10 mg cm^{-2} or 20 mg cm^{-2} respectively. Standard S cathodes were prepared by a traditional slurry coating method. S powder, super P powder, and polyvinylidene fluoride (PVDF) in a weight ratio of 5:4:1 were mixed and grounded for 30 min in N-methyl pyrrolidone (NMP) solution. The obtained slurry was cast on a piece of aluminum foil. Then the cathodes were cut into pieces with a diameter of 10 mm, and the typical areal S loading was about 2.5 mg cm^{-2}.

2.3. Preparation of CNT aerogel@S cathodes

CNT aerogel was laser-cut into cylindrical pieces with a diameter of 10 m 100 mg S was dispersed in 500 mL ethanol, and 1 mL dispersion was evenly dropped into the CNT aerogel pieces, followed by drying at 60 °C. After repeating the above operation for 10 times, a composite of CNT aerogel and S was obtained. This composite was further maintained at 155 °C for 12 h to achieve CNT aerogel@S cathode. The S areal loading and content in the cathode were 2.5 mg cm^{-2} and 33 wt%, respectively.

2.4. Assembly of coin and pouch cells

The assembly of both coin and pouch cells was performed in an argon glove box (M. Braun Inert Gas Systems Co., Ltd., Germany). Coin-type (CR 2032) half-cells were assembled with CNT aerogel@Li$_2$S$_8$ cathode as the working electrode and pure Li foil as both the counter and the reference electrode. The prepared cathodes, polypropylene separator, Li foil, stainless steel plate and spring plate are stacked in the coin cell successively. For the CNT aerogel@Li$_2$S$_8$ cathode, no additional electrolyte was added. For CNT aerogel@S and standard S cathode, an appropriate amount of electrolyte was added into the coin cell (E/S ratio = 15.6 μL mg^{-1}). All coin cells were assembled under the same pressure (10 MPa) to ensure the same thickness of the cathodes and left to activate for 48 h. For the assembly of pouch cells, the CNT aerogel was laser cut into a 2 cm × 2.4 cm piece and spot-welded with a 0.4 cm aluminum lead for use as the cathode. The anode was made by cold pressing a 2 cm × 2.4 cm lithium foil with a 0.4 cm nickel lead. A polypropylene separator was used. 305 μL Li$_2$S$_8$ solution (0.5 mol L^{-1}) was injected into the cathode before encapsulation of

the pouch cell by an aluminum-plastic film. The areal S loading was 10 mg cm^{-2}, and the E/S ratio was 7.8 μL mg^{-1}.

2.5. Morphology and structural characterization

The morphology and structure of the CNT aerogels and CNT aerogel@Li$_2$S$_8$ cathodes were characterized by scanning electron microscope (SEM, Sirion 200, FEI, USA) and transmission electron microscope (TEM, Tecnai G2F20, FEI). X-ray photoelectron spectroscopy (XPS) data of the aerogel@S cathodes were collected from a PHI Quantera II (Ulvac-Phi Inc) at room temperature. Surface area analysis was conducted using a surface area and porosity analyzer (Micromeritics ASAP 2020 HD88). Compressed CNT aerogel cathodes were used for the morphology and structural characterization to ensure that they were in similar situation as in coin cells.

2.6. Electrochemical measurements

Electrochemical measurements were carried out using a Land CT2001 automatic battery tester from 1.8 to 2.6 V at designated rates for coin cells and using a Neware battery tester from 1.6 to 2.5 V for pouch cells. The area of the electrode and the mass of the active material in pouch cells were much larger than those in coin cells, leading to greater polarization of the cell. Therefore, smaller potential window was used for pouch cells. Cyclic voltammetry (CV) tests were carried out in coin cells on a VMP-3 electrochemical workstation with a voltage range of 1.5–3.0 V and various scan rates. Electrochemical impedance spectroscopy (EIS) characterization was performed with a small perturbation voltage of 2 mV, and the frequency ranged from 100 mHz to 100 kHz. All the electrochemical tests were performed at room temperature and in an ambient atmosphere.

3. Results and discussion

The synthesis procedure of the CNT aerogel is shown in Fig. 1a. As reported in previous work, due to their clean surfaces and the strong van der Waals forces, SACNTs can self-assemble into a continuous and macroscopic CNT aerogel by a freeze-drying method [39]. First, the SACNT array was ultrasonically dispersed in ethanol and the CNT dispersion was washed with deionized water. Then, the aqueous CNT dispersion was dried to different volumes according to the required densities. Afterward, the CNT dispersion was poured into a container and underwent a freeze-drying process to obtain a CNT aerogel. The CNT aerogels with densities of 5 mg cm^{-3}, 10 mg cm^{-3}, and 20 mg cm^{-3} were laser cut into cylinders of 10 mm in diameter. The photograph of a CNT aerogel in Fig. 1b demonstrates its porous structure. SEM images in Fig. S1 show that the typical diameters of the macropores in the CNT aerogels with densities of 5 mg cm^{-3}, 10 mg cm^{-3}, and 20 mg cm^{-3} were 200 μm, 100 μm, and 50 μm respectively. The nitrogen adsorption/desorption isotherms show that all the CNT aerogels with different densities conformed to the behavior of a macroporous structure (Fig. 1c), and the observed hysteresis suggests the presence of both macropores and mesopores in the CNT aerogels. The specific surface areas of the CNT aerogels were almost identical, being 104.75 m^2 g^{-1}, 104.23 m^2 g^{-1}, and 105.11 m^2 g^{-1} for the CNT aerogels with densities of 5 mg cm^{-3}, 10 mg cm^{-3}, and 20 mg cm^{-3} respectively. The pore size distributions in Fig. 1d reveal that the mesopore sizes of the CNT aerogels with different densities were similar, with a specific mesopore volume of 0.45 cm^3 g^{-1}. The origin of the mesopores was investigated by TEM (Fig. S2). In the CNT aerogel, CNTs with a diameter of 12 nm were interwoven with each other, and the pores between adjacent CNTs constituted the mesoporous structure. The change of density of the

CNT aerogel did not have a significant impact on the size of mesopores and the variation of macroporous size with density made little contribution to the overall specific surface area of the CNT aerogels. In this work, CNT aerogels with a density of 20 mg cm^{-3} were used for subsequent experiments.

The wetting properties of the CNT aerogels were characterized. Figs. S3a and S3b show photographs of electrolyte and water droplets (20 μL) on the surfaces of the CNT aerogels. The wetting angle of electrolyte on the CNT aerogel (16.3°) was significantly smaller than that of water on the CNT aerogel (113°). The excellent wettability between the electrolyte and the CNT aerogel can facilitate sufficient ion transport channels for the assembled battery during cycling. By adding Li$_2$S$_8$ solution, the CNT aerogel@Li$_2$S$_8$ cathodes can easily reach a high areal S loading. For example, after adding 60 μL of Li$_2$S$_8$ solution (0.25 mol L^{-1}) to the CNT aerogel, the areal S loading of the CNT aerogel@Li$_2$S$_8$ cathode was 5 mg cm^{-2}. The SEM image of CNT aerogel@Li$_2$S$_8$ cathode is shown in Fig. 1e. Energy dispersive X-ray (EDX) mapping of the CNT aerogel@Li$_2$S$_8$ cathode shows that both S and carbon (C) elements were homogeneously distributed in the cathode (Fig. 1f–h), and no apparent agglomeration of S was observed. These microscopic results suggest that CNT aerogel@Li$_2$S$_8$ cathodes with uniform distribution of S have been successfully obtained, which is vital to improve the utilization of active material and the performances of the batteries. The preparation method is simple and scalable, providing a route for low-cost fabrication of S cathodes.

The cycling performances of the CNT aerogel@Li$_2$S$_8$, CNT aerogel@S, and standard S cathodes with areal S loadings of 5 mg cm^{-2}, 2.5 mg cm^{-2} and 2.5 mg cm^{-2} respectively are shown in Fig. 2a. The discharge specific capacity of the CNT aerogel@Li$_2$S$_8$ cathode was close to the theoretical capacity of S at 0.1C and maintained at 1297.2 mAh g^{-1} after 100 cycles at 0.2C. In comparison, the capacity of the CNT aerogel@S and standard S cathode decreased to only 696.5 mAh g^{-1} and 392.3 mAh g^{-1} respectively after 100 cycles at 0.2C. The volume capacities of the CNT aerogel@Li$_2$S$_8$, CNT aerogel@S, and standard S cathodes after 100 cycles at 0.2C were 720.7 Ah L^{-1}, 193.5 Ah L^{-1}, and 142.6 Ah L^{-1}. Comparison between the CNT aerogel@S and standard S cathodes with the same areal sulfur loading revealed that the CNT aerogel can effectively improve the specific capacity and cyclic stability of the S cathode due to the conductive network and rich porous structure. However, it was challenging to achieve CNT aerogel@S cathodes with high areal S loading. Herein, CNT aerogel@Li$_2$S$_8$ cathodes with ultra-high areal S loading were developed by dropping Li$_2$S$_8$ solution into the CNT aerogels. Even though the areal S loading was doubled in the CNT aerogel@Li$_2$S$_8$ cathode, it still showed much higher specific capacity and cycling stability than the standard S cathode, indicating that its unique structure could effectively improve the utilization rate of S and enhance the cycling stability. The advantages of CNT aerogel @ Li$_2$S$_8$ were further verified in the subsequent electrochemical test. The rate performances of the CNT aerogel@Li$_2$S$_8$, CNT aerogel@S, and standard S cathodes are shown in Fig. 2b. The CNT aerogel@Li$_2$S$_8$ cathode delivered specific discharge capacities of 1569.0 mAh g^{-1}, 1447.8 mAh g^{-1}, 1384.8 mAh g^{-1}, 1363.6 mAh g^{-1}, and 1268.9 mAh g^{-1} at 0.1C, 0.2C, 0.5C, 1C, and 2C, respectively. When switching back to 0.1C, the capacity recovered to 1549.2 mAh g^{-1}, reflecting its high reversibility. The CNT aerogel@S cathode showed inferior rate performance, which delivered specific discharge capacities of 971.0 mAh g^{-1}, 954.0 mAh g^{-1}, 916.3 mAh g^{-1}, 856.9 mAh g^{-1}, and 695.0 mAh g^{-1} at 0.1C, 0.2C, 0.5C, 1C, and 2C, respectively. Obvious capacity decay was observed at high rates. When switching back to 0.1C, the capacity recovered to only 968.3 mAh g^{-1}. As for the standard S cathode, a significant capacity decay was observed at 0.1C, suggesting a severe loss of active material. It showed a specific capacity of only 496.0 mAh g^{-1} at 0.2C, and
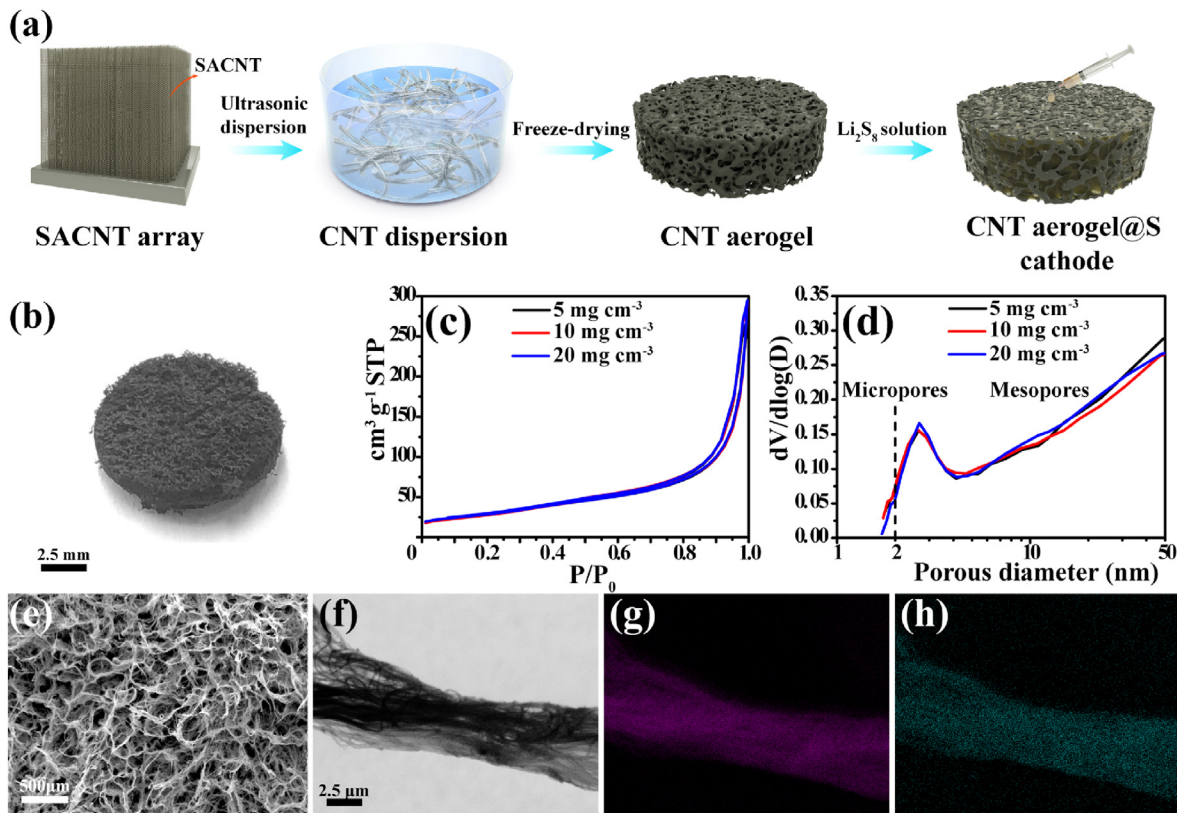
Fig. 1. (a) Schematic of the fabrication process of a CNT aerogel@Li_2S_8 cathode. (b) Digital photo of a CNT aerogel. (c) Nitrogen adsorption-desorption isotherms and (d) pore size distributions of the CNT aerogels with different densities. (e,f) SEM images of a CNT aerogel@Li_2S_8 cathode. (g) Carbon and (h) sulfur elemental mapping of (f). (A colour version of this figure can be viewed online.)

almost no capacity released at 0.5C or higher rate. After cycling at 1C and 2C, when the working current decreased to 0.1C, the specific capacity recovered to only 491.9 mAh g^{-1}. Overall, the CNT aerogel@Li_2S_8 cathode showed superior cycling and rate performances than the standard S cathode, due to the unique characteristics of 3D porous microstructures of the CNT aerogel. The coulombic efficiencies of the cathodes in the rate tests are shown in Fig. S4. The standard S cathode exhibited the lowest coulombic efficiency, while the coulombic efficiencies of the CNT aerogel-based cathodes remain above 95%. There is no obvious difference between the CNT aerogel@Li_2S_8 and CNT aerogel@S cathodes. These results suggest that the introduction of the CNT aerogel has a significant effect on the suppression of the shuttle effect.

The differences between the charging and discharging platforms (ΔE) in the voltage-capacity curves of the CNT aerogel@Li_2S_8, CNT aerogel@S and standard S cathodes were evaluated (Fig. 2c). ΔE of the CNT aerogel@Li_2S_8 cathode was only 0.26 V, much smaller than that of the CNT aerogel@S (0.33 V) and standard S (0.53 V) cathodes. The smaller ΔE value of the CNT aerogel@Li_2S_8 cathode suggests its smaller polarization and better electrochemical reversibility. The EIS results of coin cells after activation process (SOC = 1) in Fig. 2d show much lower impedance characteristic of the CNT aerogel@Li_2S_8 cathode compared to other S cathodes. The equivalent circuits of the impedance spectra and results of fitting are shown in Fig. S5 and Table 1, respectively. The ohmic resistance of the CNT aerogel@Li_2S_8 cathode was 2.5 Ω, which was higher than that of the CNT aerogel@S (2.3 Ω) and standard S (1.1 Ω) cathodes. Because Li_2S_8 solution was used as the initial active material in the CNT aerogel@Li_2S_8 cathode, the overall concentration of the solution was higher than that of the pure electrolyte used in the

standard S cathode, resulting in higher ohmic resistance in the CNT aerogel@Li_2S_8 cathode. In the standard S cathode, additional conductive agent (Super-P) was used. The surfaces of S particles were coated by a conductive carbon layer, and the ohmic resistance of the standard S cathode was slightly smaller than the CNT aerogel@S cathode. In the low-frequency region, all cathodes showed a sloped line related to the Warburg diffusion process. The CNT aerogel@Li_2S_8 cathode exhibited a unique semicircle (R_2~ 1.1 Ω) in the low-frequency region because a new charge transfer interface was generated with Li_2S_8 as the initial active material. In the high-frequency region, both cathodes exhibited semicircles corresponding to the charge transfer resistance (R_1). As shown in Table S1, the R_1 between CNTs and Li_2S_8 in the CNT aerogel@Li_2S_8 cathode was only 7.7 Ω, which was much smaller than that between Super-P and S in the standard S cathode (175.5 Ω). It was worth noting that the charge transfer resistance of the CNT aerogel@S cathode was also lower than that of the standard S cathode, revealing that the CNT aerogel plays an important role in improving ion diffusion. The significantly lower impedance of the CNT aerogel@Li_2S_8 cathode indicates its faster reaction kinetics, which is ascribed to the 3D conductive network to ensure sufficient electron transfer and the good wettability between the electrolyte and the porous structure to facilitate fast lithium-ion transport.

The CV curves of the CNT aerogel@Li_2S_8 and standard S cathodes at a scanning rate of 0.1 mV s^{-1} display two-step redox reactions during the lithiation/delithiation processes of S, involving two cathodic reduction peaks and continuous anodic oxidation peak (Fig. S6). Two reduction peaks corresponded to the reduction of S to polysulfides and the reduction of polysulfides to Li_2S_2/Li_2S, respectively. The oxidation peaks represented the oxidation
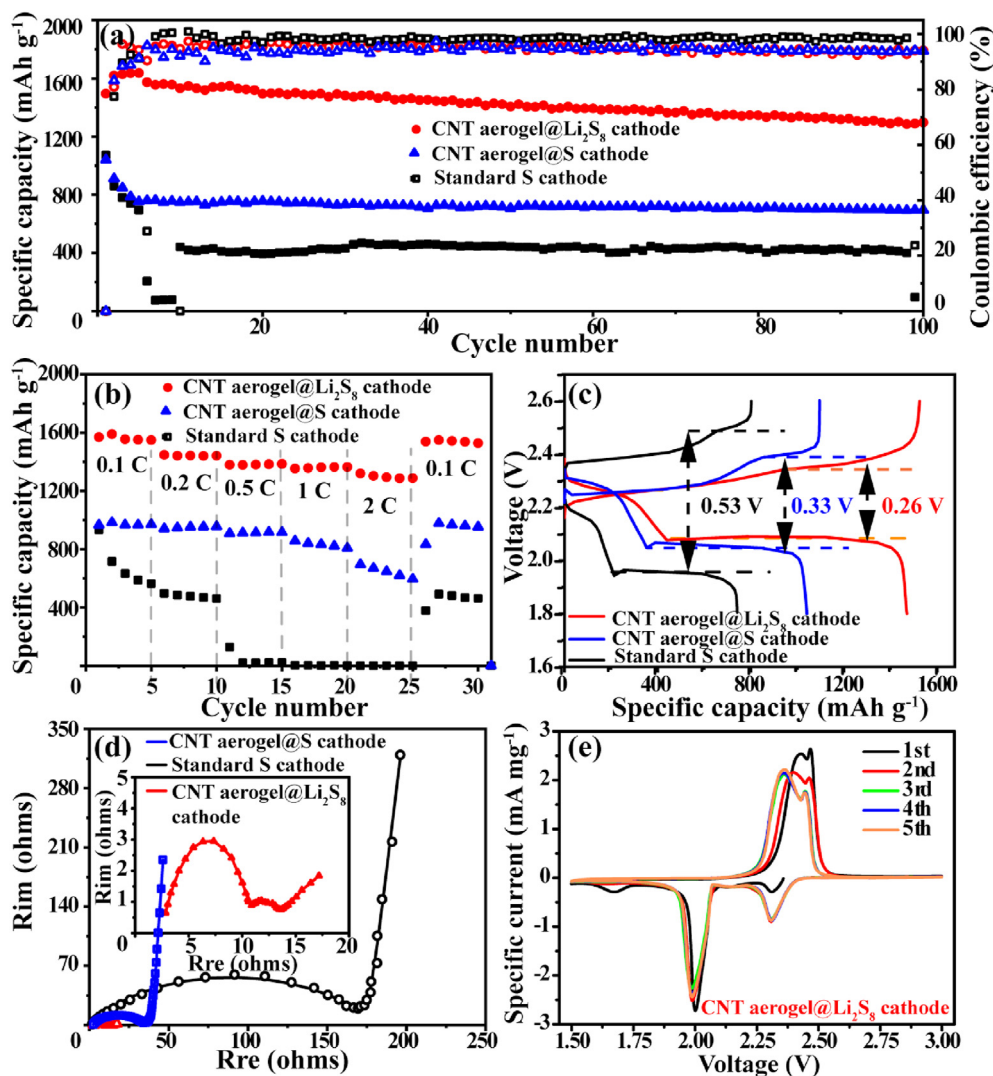
Fig. 2. Electrochemical performances of the CNT aerogel@Li$_2$S$_8$, CNT aerogel@S and standard S cathodes. (a) Cycling performances at 0.2C. (b) Rate performances. (c) Voltage profiles. (d) EIS analysis. (e) CV curves. (A colour version of this figure can be viewed online.)

Table 1
EIS fitting data of the standard S, CNT aerogel@S, and CNT aerogel@Li$_2$S$_8$ cathodes.

Sample	R$_0$	R$_1$	R$_2$
Standard S cathode	1.1 Ω	175.5 Ω	/
CNT aerogel@S cathode	2.3 Ω	33.2 Ω	/
CNT aerogel@Li$_2$S$_8$ cathode	2.5 Ω	7.7 Ω	1.1 Ω

reaction from Li$_2$S$_2$/Li$_2$S to Li$_2$S$_8$/S [42]. The CNT aerogel@Li$_2$S$_8$ cathode showed sharper and symmetric redox peaks corresponding to relatively smaller polarization and superior electrochemical kinetics of the cathode compared to those of the other S cathode. Fig. 2e shows the CV curve of the CNT aerogel@Li$_2$S$_8$ cathode during the first 5 cycles. Two reduction peaks at 2.3 V and 2.0 V corresponded to the reduction of S to polysulfides and the reduction of polysulfides to Li$_2$S$_2$/Li$_2$S, respectively. An additional reduction peak around 1.65 V during the first cycle corresponded to the decomposition of LiNO$_3$ [43], and this peak was no longer observed in the subsequent cycles. The oxidation peaks represented the oxidation reactions from Li$_2$S$_2$/Li$_2$S to Li$_2$S$_8$/S. The curves hardly changed after the third cycle, indicating the excellent electrochemical and structural stability of the CNT aerogel@Li$_2$S$_8$ cathode. These

electrochemical testing results suggest that high S utilization, low polarization, and fast reaction kinetics were achieved in the CNT aerogel@Li$_2$S$_8$ cathode due to its 3D conductive network structure. The cycle performance of the CNT aerogel@Li$_2$S$_8$ cathode at 1C is shown in Fig. S7. The CNT aerogel@Li$_2$S$_8$ cathode exhibited an ultra-high specific capacity of 1388.2 mAh g^{-1} and maintained 899.9 mAh g^{-1} after 60 cycles, and the coulombic efficiency remained above 97%, indicating that the shuttle effect was effectively suppressed.

For Li—S batteries with polysulfides as the initial active material, the active material generally undergoes the following process: During the initial discharge-charging process, the polysulfides firstly discharge to Li$_2$S$_2$/Li$_2$S, and then convert to S$_8$ by recharging. After the second cycle, the conversion process of the active material in the Li—S battery is S$_8$—polysulfides—Li$_2$S$_2$/Li$_2$S, which is consistent with the standard S cathode [44]. The morphology changes of the active material on the CNT surface in the CNT aerogel@Li$_2$S$_8$ cathode under different charging and discharging states was also observed. First, the CNT aerogel@Li$_2$S$_8$ cathode was assembled into coin cells. Then, the cathodes were disassembled from the coin cells at various stages: the initial state, after the first discharge to 1.8V (0.1C), and recharge to 2.6 V (0.1C) after discharging, then

characterized by SEM (Fig. S8). Fig. S8a showed the CNT aerogel@Li_2S_8 cathode at the initial state. Li_2S_8 particles were evenly distributed among the CNTs. When the cathode was discharged to 1.8 V, Li_2S_8 converted to Li_2S_2/Li_2S particles that were uniformly deposited on the surface of CNTs (Fig. S8b). The pores formed by the interweaving CNTs firmly restricted the Li_2S_2/Li_2S particles in the cathode, illustrating that the CNT aerogel can effectively inhibit the shuttling of polysulfides. When the cathode was recharged to 2.6V, Li_2S_2/Li_2S converted to S_8 particles that evenly coated on the surface of CNTs (Fig. S8c), which was beneficial to prompt the utilization rate of S and obtain a higher capacity and cycle stability.

Conditions of the separators were examined to study the stability of the cathodes during cycling. Fig. S9 shows digital photos of the original separator and the separators used in the cells with the CNT aerogel@Li_2S_8 and standard S cathodes after 100 cycles. The separator in the cell with the CNT aerogel@Li_2S_8 cathode still looked as white as the original separator after 100 cycles. In comparison, the separator used in the cell with the standard S cathode clearly showed yellow residue, suggesting the presence of polysulfides on the separator. The absence of polysulfides residue on the separator in the cell with the CNT aerogel@Li_2S_8 cathode indicated that such cathode had a strong restrictive effect on the polysulfides shuttling, which is beneficial to the cycling stability of the batteries, and the mechanism for the CNT aerogels to suppress the shuttle effect was further investigated. The most basic argument is whether the restriction of CNT aerogels on polysulfides is physical or chemical effect. To verify this dispute, the CNT aerogel was immersed in Li_2S_8 and Li_2S_4 solution for 24 h, then dried and subjected to an XPS test. Fig. S10 shows the spectrum of C 1s, in which only two peaks were observed after soaking the CNT aerogels in Li_2S_8 and Li_2S_4 solutions. One peak at 284.8 eV corresponded to the binding energy of the C—C bond in CNTs, and the other peak at 288.1 eV represented that of the C—F bond of in LiTFSI. No other peak was observed, indicating that the restriction effect of the CNT aerogels on polysulfides was mainly physical adsorption rather than chemical adsorption.

Based on the XPS results and structural characteristics of the CNT aerogel, the principle of the polysulfide adsorption by the CNT aerogel is proposed in Fig. 3a. The mesopores eventually absorbed the Li_2S_8 solution in the CNT aerogel through three steps. In the first step, the Li_2S_8 solution was dropped into the CNT aerogel and primitively entered the macropores. In the second step, the Li_2S_8 solution was rapidly absorbed from the macropore into the mesopores with a "capillary tube" structure formed between interwoven CNTs in the CNT aerogel. When the Li_2S_8 solution was completely absorbed into the mesopores, a stable state was achieved. In this final step, the electrolyte was firmly confined in the mesopores. To verify the principle of polysulfide adsorption by the CNT aerogel, two critical issues needed to be probed: (i) Does the porous structure in the CNT aerogel prevent polysulfide shuttling when Li_2S_8 solution was absorbed entirely? (ii) Whether macropores or mesopores play a significant role in this capillary action?

Polysulfides dissolution tests were performed to study whether the porous structure in the CNT aerogel can effectively confine polysulfides in the cathode and suppress the shuttle effect (Fig. 3b). First, the coin cells of the CNT aerogel @S and the standard S cathodes were assembled, and their voltage profiles during the first discharge process are shown in Fig. 3c. The initial voltages of the second discharge platforms for the CNT aerogel @S and the standard S cathodes were 2.09 V and 1.95 V, respectively. At these voltages, the polysulfides in these cells had the highest concentration and the most similar electrolyte composition. Therefore, the CNT aerogel @S and the standard S cathodes were discharged to 2.09 V and 1.95 V at 0.1C, respectively, then disassembled in an argon-filled glove box and put into containers with 3 mL pure

electrolyte. The color changes of the electrolyte are shown in Fig. 3b. When the standard S cathode was immersed in the electrolyte, the polysulfides in the cathode diffused rapidly into the electrolyte and the color of the electrolyte quickly turned light chartreuse, indicating that the polysulfides produced during the charge and discharge processes were not effectively confined in the standard S cathode. In comparison, when the CNT aerogel@Li_2S_8 cathode was placed in the electrolyte, the color of the electrolyte maintained a relatively clear state. After standing for 1 h, color gradient appeared in the electrolyte, and the electrolyte close to the CNT aerogel@Li_2S_8 cathode looked darker than other locations, as the polysulfides that were initially confined in the porous structure of the CNT aerogel slowly diffused into the electrolyte. After standing for 2 h, the polysulfides in the CNT aerogel completely diffused throughout the electrolyte, and the solution finally appeared light chartreuse. The much slower diffusion of polysulfides from the CNT aerogel into the electrolyte compared to the standard S cathode suggests that the porous structure of the CNT aerogel can better confine the polysulfides in the cathode to alleviate the shuttle effect.

Whether the macropores or mesopores in the CNT aerogels play a significant role in the capillary action and the suppression of polysulfide diffusion was also investigated. Three kinds of CNT aerogels with densities of 5 mg cm^{-3}, 10 mg cm^{-3}, and 20 mg cm^{-3} possessed different macropore sizes but similar mesoporous structures. They were used to prepare coin cells for electrochemical and cyclic tests, and the corresponding CNT aerogel@Li_2S_8 cathodes demonstrated almost the same EIS, CV, and cycling performances (Fig. 3d—f). Therefore, the macropores in the CNT aerogels did not affect their electrochemical performances. It is the mesopores that do not vary with density in the CNT aerogels plays a significant role in alleviating the polysulfide shuttle effect.

The polysulfide dissolution test results and electrochemical performances of CNT aerogels with different densities suggest that the mesoporous structure in the CNT aerogel can absorb Li_2S_8 solution through capillary action and restrict the polysulfide shuttling. Furthermore, the processes of Li_2S_8 solution absorption and confinement in the mesopores were simulated by multiphysics simulation (Fig. 3g). According to the microstructure of the CNT aerogel, a two-dimensional (2D) cross-section model containing both macropores and mesopores was constructed. In the simulation model, three mesoporous rectangular cross sections with a pore diameter of 30 nm were constructed by four CNTs with a diameter of 12 nm and a length of 500 nm. Two rectangular argon-filled regions with a cross section of 600 nm in length and 80 nm in height were set above and below the mesopores to simulate the macropores connected to the mesopores. In addition, there was an appropriate amount of electrolyte, specifically a rectangular cross section of 250 nm in length and 80 nm in height, below the mesopores used to simulate the Li_2S_8 solution that first entered the macropores in the CNT aerogel. The surface tension of the electrolyte and the wetting angle between the electrolyte and the CNT aerogel were also taken into account. The surface pressure and the distribution of the electrolyte in the entire model structure were simulated. In the initial state, the entire electrolyte was underneath the mesopores. The upper surface of the electrolyte underneath the mesopores showed a negative pressure due to the capillary action and the electrolyte tended to enter the mesopores. After 0.5 μs, most of the electrolyte entered the mesopores, and the upper surface of the electrolyte in the mesopores still maintained a high negative pressure, making the electrolyte continue to fill the mesopores. After 1 μs, the electrolyte that was previously in the macropores entered the mesopores entirely, but the mesopores were still not totally filled. The electrolyte in the mesopores showed negative pressure. After 2 μs, the mesopores was totally filled by the
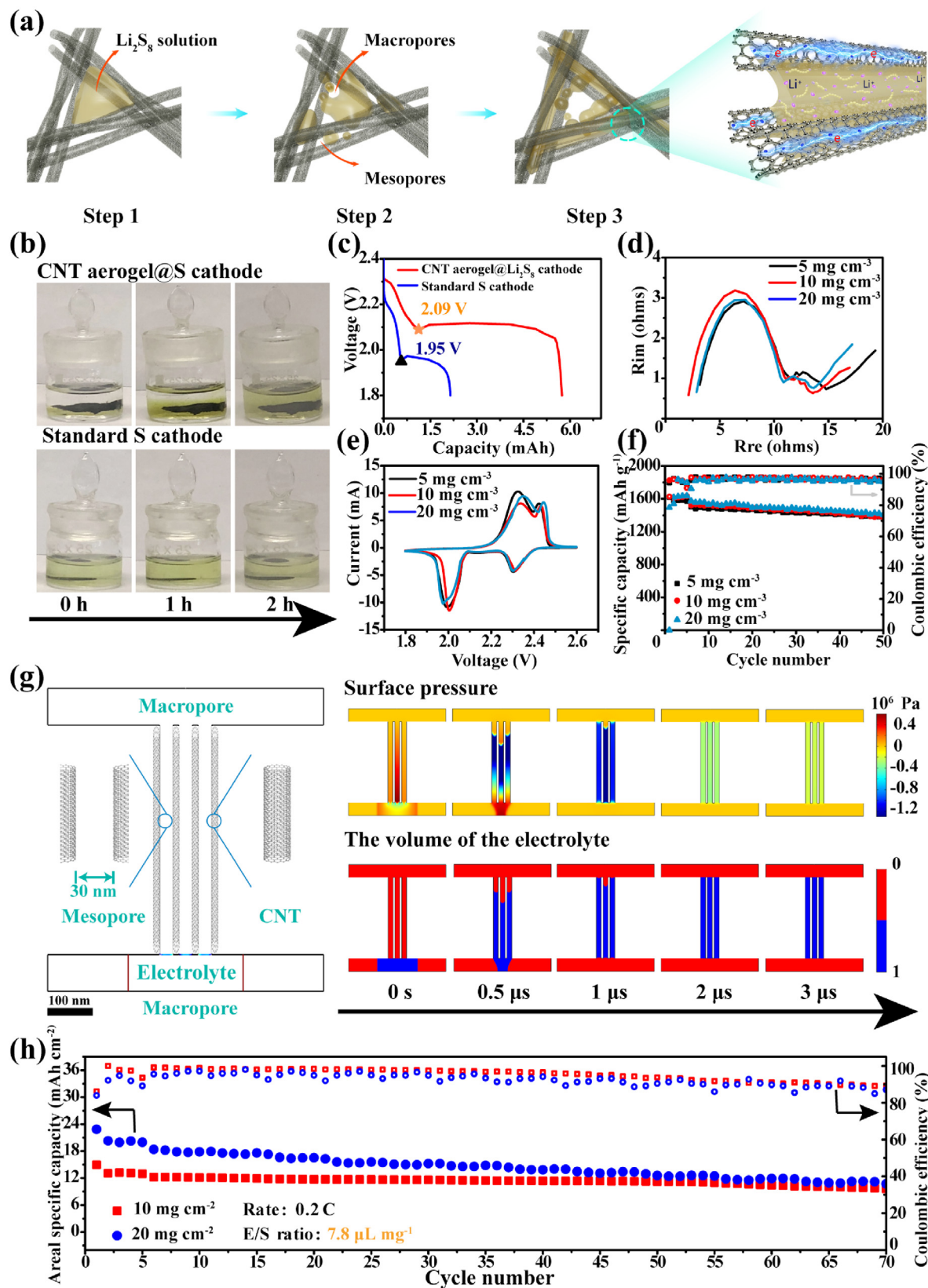
Fig. 3. (a) Schematic of the CNT aerogel@Li$_2$S$_8$ cathode absorbing Li$_2$S$_8$ solution and confining polysulfides. (b) Color changes of the electrolyte with immersion of the CNT aerogel@Li$_2$S$_8$ and standard S cathodes after a discharge process. (c) Voltage profiles of the CNT aerogel@Li$_2$S$_8$ and standard S cathodes during the first discharge process extracted from Fig. 2c. (d–f) EIS spectra, CV curves, and cycling performances of CNT aerogel@Li$_2$S$_8$ cathodes using CNT aerogels with densities of 5, 10, and 20 mg cm^{-3}. (g) Multiphysics simulation of the electrolyte absorption by the CNT aerogel. (h) Areal specific capacities of CNT aerogel@Li$_2$S$_8$ cathodes with high S loading at 0.2C. (A colour version of this figure can be viewed online.)
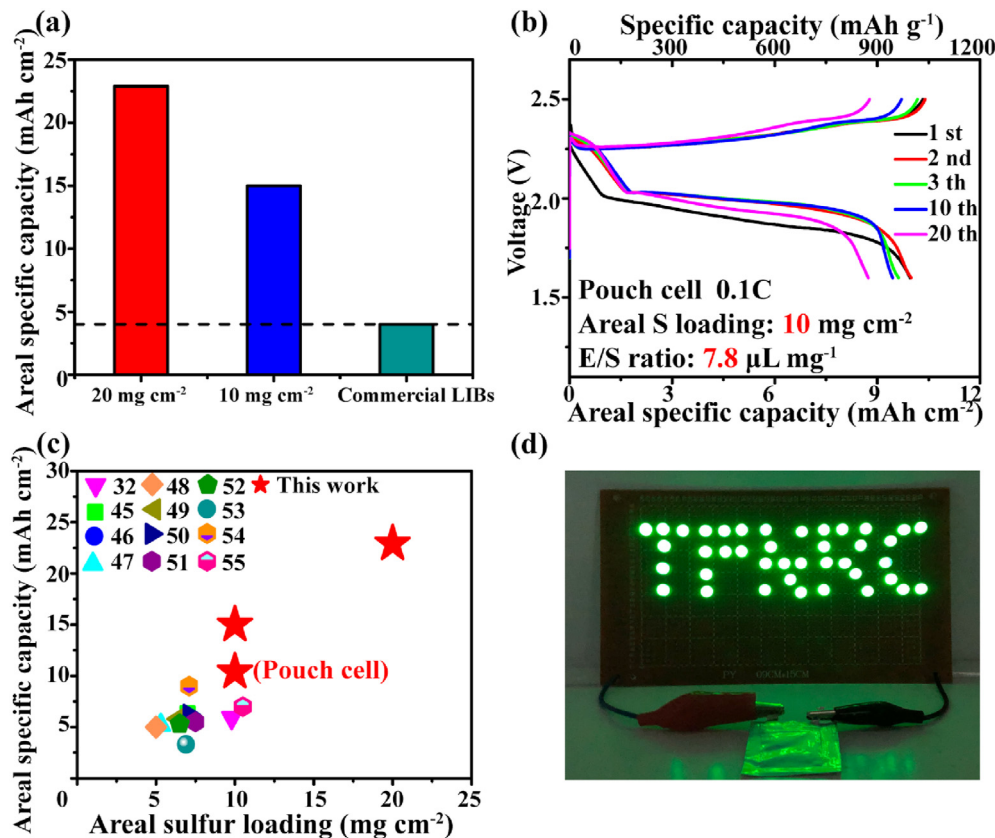
Fig. 4. (a) Areal specific capacities of the CNT aerogel@Li_2S_8 cathodes with high S loadings compared to commercial LIBs. (b) Charge and discharge curves of a CNT aerogel@Li_2S_8 pouch cell at 0.1C. (c) Comparison of the areal specific capacities of the CNT aerogel@Li_2S_8 with data reported in the literature. (d) A green LED array illuminated by a CNT aerogel@Li_2S_8 pouch cell. (A colour version of this figure can be viewed online.)

electrolyte, which maintained a small negative pressure to prevent the electrolyte from flowing out. At this moment, a steady state was reached and remained unchanged afterward. These simulation results sufficiently proved that the CNT aerogel absorbed the Li_2S_8 solution into the mesopores by capillary action and stably restricted the polysulfides in the cathode, as shown in Fig. 3a. The stable negative pressure state formed in a short time can adsorb and restrict the polysulfide solution in the mesopores, and thus effectively improve specific capacity, rate performance, and cycle stability of the CNT aerogel@Li_2S_8 cathodes: On the one hand, more Li_2S_8 active materials can directly contact the conductive network composed of CNTs and the ion channels provided by the electrolyte, which improves the utilization of active materials and accelerates reaction kinetics; On the other hand, due to the strong capillary action, the polysulfides generated during the charging and discharging processes are firmly confined by the mesopores in the cathode, which inhibits the polysulfide shuttle effect and improves cycle stability of the cathode.

Due to the above-mentioned unique characteristics of the CNT aerogel@Li_2S_8 cathodes, the areal S loading can be significantly increased to 10 mg cm^{-2} and 20 mg cm^{-2}, and the electrolyte S ratio can be reduced to 7.8 μL mg^{-1} to fulfill the needs for industrial applications. Cycling performances of the CNT aerogel@Li_2S_8 cathodes with high areal S loadings (10 mg cm^{-2} and 20 mg cm^{-2}) are demonstrated in Fig. 3h. With an areal S loading of 10 mg cm^{-2}, the initial areal specific capacity of CNT aerogel@Li_2S_8 cathode reached 15.0 mAh cm^{-2} and still maintained 9.6 mAh cm^{-2} after 70 cycles at 0.2C. When the areal S loading increased to 20 mg cm^{-2}, the CNT aerogel@Li_2S_8 cathode still demonstrated a high areal specific

capacity of 22.9 mAh cm^{-2} and maintained capacities of 10.7 mAh cm^{-2} after 70 cycles at 0.2C. Fig. 4a is a more straightforward bar chart showing the extremely high areal specific capacity and cyclic stability of the CNT aerogel@Li_2S_8 cathode with high S loading. Li−S batteries prepared by the CNT aerogel@Li_2S_8 cathodes can have an areal specific capacity up to more than 5 times of that of commercial LIBs, indicating that their remarkable potential in practical applications.

To further illustrate the suitability of the CNT aerogel@Li_2S_8 cathodes for industrial applications, a large size pouch cell was prepared with an areal S loading of 10 mg cm^{-2} and an electrolyte S ratio of 7.8 μL mg^{-1}. The cycling performance of the pouch cell at 0.1C is shown in Fig. 4b. It exhibited a high areal specific capacity of 10.4 mAh cm^{-2} and excellent cycling stability, with the areal specific capacity remaining at 8.8 mAh cm^{-2} after 20 cycles. Compared with data reported in the literature [45−55], the CNT aerogel@Li_2S_8 cathode in this work has higher areal S loading and specific capacity (Fig. 4c), indicating that its unique porous aerogel structure and capillary action can significantly improve the performance of Li−S batteries. Fig. 4d shows that a pouch cell made with a CNT aerogel@Li_2S_8 cathode illuminated a green LED array with a "TFNRC" pattern representing Tsinghua-Foxconn Nanotechnology Research Center, illustrating the possibility of using the pouch cell for high-energy-density Li−S batteries.

4. Conclusion

In this work, 3D porous CNT aerogels were prepared by a simple freeze-drying method. Due to the rich mesoporous structures in the

CNT aerogel and its good wettability to the electrolyte, these mesopores had an extremely strong capillary action on the electrolyte. When the Li_2S_8 solution formed by dissolving Li_2S_8 in the electrolyte as the initial active material was added to the CNT aerogel, the Li_2S_8 solution was absorbed into the mesopores entirely and maintained a stable negative pressure state within a short time (2 μs). On the one hand, the rapid absorption of Li_2S_8 solution by mesopores significantly improved the utilization of active materials, and an ultrahigh areal S loading and specific capacity can be achieved by adjusting the volume or concentration of the Li_2S_8 solution. On the other hand, the stable negative pressure state of the electrolyte in the mesopores restricted the polysulfides in the mesopores of the cathode, which enhanced the cycle stability. Based on the mesoporous structure of the CNT aerogel and the intense capillary action asserted on the electrolyte, the performances of Li—S batteries assembled by CNT aerogel@Li_2S_8 cathodes were effectively improved. Especially when the E/S ratio was reduced to 7.8 μL mg^{-1} and the areal S loadings were increased to 20 mg cm^{-2}, the CNT aerogel@Li_2S_8 cathode still showed an ultrahigh areal capacity of 22.9 mAh cm^{-2}. Furthermore, the initial areal specific capacity of a large scale pouch cell made with the CNT aerogel@Li_2S_8 cathode reached as high as 10.4 mAh cm^{-2}, showing the great potential for the CNT aerogel-based cathodes in practical applications of Li—S systems.

Declaration of competing interest

The authors declare that they have no known competing financial interests or personal relationships that could have appeared to influence the work reported in this paper.

CRediT authorship contribution statement

Zhenhan Fang: Conceptualization, Investigation, Writing - original draft. **Yufeng Luo:** Conceptualization, Investigation, Writing - original draft. **Hengcai Wu:** Investigation. **Lingjia Yan:** Investigation. **Fei Zhao:** Investigation. **Qunqing Li:** Conceptualization, Supervision. **Shoushan Fan:** Conceptualization, Supervision. **Jiaping Wang:** Conceptualization, Supervision, Writing - review & editing.

Acknowledgments

Appendix A. Supplementary data

Supplementary data to this article can be found online at https://doi.org/10.1016/j.carbon.2020.05.047.

References

[1] R. Van Noorden, A better battery, Nature 507 (7490) (2014) 26—28, https://doi.org/10.1038/507026a.

[2] M. Armand, J.M. Tarascon, Building better batteries, Nature 451 (2008) 652—657, https://doi.org/10.1038/451652a.

[3] N. Nitta, F.X. Wu, J.T. Lee, G. Yushin, Li-ion battery materials: present and future, Mater. Today 18 (2015) 252—264, https://doi.org/10.1016/j.mattod.2014.10.040.

[4] A. Manthiram, Y.Z. Fu, S.H. Chung, C.X. Zu, Y.S. Su, Rechargeable lithium-sulfur batteries, Chem. Rev. 114 (2014) 11751—11787, https://doi.org/10.1021/cr500062v.

[5] X. Ji, L.F. Nazar, Advances in Li—S batteries, J. Mater. Chem. 20 (2010) 9821—9826, https://doi.org/10.1039/B925751A.

[6] M. Wild, L. O'Neill, T. Zhang, R. Purlayastha, G. Minton, M. Marinescu, et al., Lithium sulfur batteries, a mechanistic review, Energy Environ. Sci. 8 (12) (2015) 3477—3494, https://doi.org/10.1039/C5EE01388G.

[7] L. Sun, D. Wang, Y. Luo, K. Wang, W. Kong, Y. Wu, et al., Sulfur embedded in mesoporous carbon nanotube network as a binder-free electrode for high performance lithium sulfur batteries, ACS Nano 10 (2016) 1300—1308, https://doi.org/10.1021/acsnano.5b06675.

[8] L. Sun, W. Kong, Y. Jiang, H. Wu, K. Jiang, J. Wang, et al., Super-aligned carbon nanotube/graphene hybrid materials as framework for sulfur cathodes in high performance lithium sulfur batteries, J. Mater. Chem. A 3 (2015) 5305—5312, https://doi.org/10.1039/C4TA06255H.

[9] S.H. Chung, A. Manthiram, A polyethylene glycol-supported microporous carbon coating as a polysulfide trap for utilizing pure sulfur cathodes in lithium-sulfur batteries, Adv. Mater. 26 (43) (2014) 7352—7357, https://doi.org/10.1002/adma.201402893.

[10] K. Yang, Q. Gao, Y. Tan, W. Tian, W. Qian, L. Zhu, et al., Biomass-derived porous carbon with micropores and small mesopores for high-performance lithium-sulfur batteries, Chem. Eur J. 22 (10) (2016) 3239—3244, https://doi.org/10.1002/chem.201504672.

[11] G. Li, J. Sun, W. Hou, S. Jiang, Y. Huang, J. Geng, Three-dimensional porous carbon composites containing high sulfur nanoparticle content for high-performance lithium-sulfur batteries, Nat. Commun. 7 (2016) 10601, https://doi.org/10.1038/ncomms10601.

[12] X. Tao, X. Chen, Y. Xia, H. Huang, Y. Ga, R. Wu, et al., Highly mesoporous carbon foams synthesized by a facile, cost-effective and template-free pechini method for advanced lithium-sulfur batteries, J. Mater. Chem. A 1 (10) (2013) 3295—3301, https://doi.org/10.1039/C2TA01213H.

[13] Z. Sun, S. Wang, L. Yan, M. Xiao, D. Han, Y. Meng, Mesoporous carbon materials prepared from litchi shell as sulfur encapsulator for lithium-sulfur battery application, J. Power Sources 324 (2016) 547—555, https://doi.org/10.1016/j.powsour.2016.05.122.

[14] S.K. Park, J. Lee, T. Hwang, B. Jang, Y. Piao, Scalable synthesis of honeycomblike ordered mesoporous carbon nanosheets and their application in lithium-sulfur batteries, ACS Appl. Mater. Interfaces 9 (3) (2017) 2430—2438, https://doi.org/10.1021/acsami.6b13370.

[15] L. Zhang, H. Huang, Y. Xia, C. Liang, W. Zhang, J. Luo, et al., High-content of sulfur uniformly embedded in mesoporous carbon: a new electrodeposition synthesis and an outstanding lithium-sulfur battery cathode, J. Mater. Chem. A 5 (12) (2017) 5905—5911, https://doi.org/10.1039/C7TA00328E.

[16] X. Yuan, B. Liu, J. Xu, X. Yang, K. Zeinu, X. He, et al., Lamellar mesoporous carbon derived from bagasse for the cathode materials of lithium-sulfur batteries, RSC Adv. 7 (22) (2017) 13595—13603, https://doi.org/10.1039/C6RA26531F.

[17] H.M. Kim, J.Y. Hwang, A. Manthiram, Y.K. Sun, High-performance lithium sulfur batteries with a self-assembled multiwall carbon nanotube interlayer and a robust electrode-electrolyte interface, ACS Appl. Mater. Interfaces 8 (1) (2016) 983—987, https://doi.org/10.1021/acsami.5b10812.

[18] Y.C. Jeong, K. Lee, T. Kim, J.H. Kim, J. Park, Y.S. Cho, et al., Partially unzipped carbon nanotubes for high-rate and stable lithium-sulfur batteries, J. Mater. Chem. A 4 (3) (2016) 819—826, https://doi.org/10.1039/C5TA07818K.

[19] J.S. Lee, J. Jun, J. Jang, A. Manthiram, Sulfur-immobilized, activated porous carbon nanotube composite based cathodes for lithium-sulfur batteries, Small 13 (12) (2017) 1602984, https://doi.org/10.1002/smll.201602984.

[20] K. Mi, Y. Jiang, J. Feng, Y. Qian, S. Xiong, Hierarchical carbon nanotubes with a thick microporous wall and inner channel as efficient scaffolds for lithium-sulfur batteries, Adv. Funct. Mater. 26 (10) (2016) 1571—1579, https://doi.org/10.1002/adfm.201504835.

[21] J.Q. Huang, X.F. Liu, Q. Zhang, C.M. Chen, M.Q. Zhao, S.-M. Zhang, et al., Entrapment of sulfur in hierarchical porous graphene for lithium-sulfur batteries with high rate performance from -40 to 60 °C, Nanomater. Energy 2 (2) (2013) 314—321, https://doi.org/10.1016/j.nanoen.2012.10.003.

[22] G. Zhou, S. Pei, L. Li, D.W. Wang, S. Wang, K. Huang, et al., A graphene -pure -sulfur sandwich structure for ultrafast, long-life lithium-sulfur batteries, Adv. Mater. 26 (4) (2014) 625—631, https://doi.org/10.1002/adma.201302877.

[23] J. Wang, Y. Yang, F. Kang, Porous carbon nanofiber paper as an effective interlayer for high-performance lithium-sulfur batteries, Electrochim. Acta 168 (2015) 271—276, https://doi.org/10.1016/j.electacta.2015.04.055.

[24] R. Singhal, S.H. Chung, A. Manthiram, V. Kalra, A free-standing carbon nano-fiber interlayer for high-performance lithium-sulfur batteries, J. Mater. Chem. A 3 (8) (2015) 4530—4538, https://doi.org/10.1039/C4TA06511E.

[25] J.S. Lee, W. Kim, J. Jang, A. Manthiram, Sulfur-embedded activated multi-channel carbon nanofiber composites for long-life, high-rate lithium sulfur batteries, Adv Energy Mater 7 (5) (2017) 1601943, https://doi.org/10.1002/aenm.201601943.

[26] X.Q. Zhang, D. Xie, D. Wang, T. Yang, X. Wang, X. Xia, et al., Carbon fiber-incorporated sulfur/carbon ternary cathode for lithium-sulfur batteries with enhanced performance, J. Solid State Electrochem. 21 (4) (2017) 1203—1210, https://doi.org/10.1007/s10008-016-3460-8.

[27] J. Song, Z. Yu, M.L. Gordin, D. Wang, Advanced sulfur cathode enabled by highly crumpled nitrogen-doped graphene sheets for high-energy density lithium-sulfur batteries, Nano Lett. 16 (2) (2016) 864—870, https://doi.org/10.1021/acs.nanolett.5b03217.

[28] C. Hu, C. Kirk, Q. Cai, C. Cuadrado-Collados, J. Silvestre-Albero, F. Rodrigurzs-Reinoso, et al., A high-volumetric-capacity cathode based on interconnected close-packed N-doped porous carbon nanospheres for long-life lithium-sulfur batteries, Adv. Energy. Mater 7 (22) (2017) 1701082, https://doi.org/10.1002/aenm.201701082.

[29] D. Su, M. Cortie, G. Wang, Fabrication of N-doped graphene-carbon nanotube hybrids from prussian blue for lithium-sulfur batteries, Adv. Energy. Mater 7 (8) (2017) 1602014, https://doi.org/10.1002/aenm.201602014.

[30] X. Yuan, B. Liu, H. Hou, K. Zeinu, Y. He, X. Yang, et al., Facile synthesis of mesoporous graphene platelets with in situ nitrogen and sulfur doping for lithium sulfur batteries, RSC Adv. 7 (36) (2017) 22567–22577, https://doi.org/10.1039/C7RA01946G.

[31] Y. Zhang, K. Sun, L. Zhan, Y. Wang, L. Ling, N-doped yolk-shell hollow carbon sphere wrapped with graphene as sulfur host for high-performance lithium-sulfur batteries, Appl. Surf. Sci. 427 (2018) 823–829, https://doi.org/10.1016/j.apsusc.2017.06.288.

[32] G. Hu, C. Xu, Z. Sun, S. Wang, H.M. Cheng, F. Li, et al., 3D graphene-foam−reduced-graphene-oxide hybrid nested hierarchical networks for high-performance Li−S batteries, Adv. Mater. 28 (2016) 1603–1609, https://doi.org/10.1002/adma.201504765.

[33] Z. Li, J.T. Zhang, Y.M. Chen, J. Li, X.W. Lou, Pie-like electrode design for high-energy density lithium−sulfur batteries, Nat. Commun. 6 (2015) 8850, https://doi.org/10.1038/ncomms9850.

[34] W. Zhou, B. Guo, H. Gao, J.B. Goodenough, Low-cost higher loading of a sulfur cathode, Adv. Energy. Mater 6 (2016) 1502059, https://doi.org/10.1002/aenm.201502059.

[35] K. Jiang, Q. Li, S. Fan, Nanotechnology: spinning continuous carbon nanotube yarns—carbon nanotubes weave their way into a range of imaginative macroscopic applications, Nature 419 (6909) (2002) 801, https://doi.org/10.1038/419801a.

[36] K. Wang, S. Luo, Y. Wu, X. He, F. Zhao, J. Wang, et al., Super-aligned carbon nanotube films as current collectors for lightweight and flexible lithium ion batteries, Adv. Funct. Mater. 23 (2013) 846–853, https://doi.org/10.1002/adfm.201202412.

[37] K. Wang, Y. Wu, H. Wu, Y. Luo, D. Wang, K. Jiang, et al., Super-aligned carbon nanotube films with a thin metal coating as highly conductive and ultralight current collectors for lithium-ion batteries, J. Power Sources 351 (2017) 160–168, https://doi.org/10.1016/j.jpowsour.2017.03.081.

[38] S. Luo, K. Wang, J. Wang, K. Jiang, Q. Li, S. Fan, Binder free LiCoO2/carbon nanotube cathodes for high-performance lithium ion batteries, Adv. Mater. 24 (2012) 2294–2298, https://doi.org/10.1002/adma.201104720.

[39] S. Luo, Y. Luo, H. Wu, M. Li, L. Yan, K. Jiang, et al., Self-assembly of 3D carbon nanotube sponges: a simple and controllable way to build macroscopic and ultralight porous architectures, Adv. Mater. 29 (2017) 1603549, https://doi.org/10.1002/adma.201603549.

[40] Y. Luo, K. Wang, S. Luo, F. Zhao, H. Wu, K. Jiang, et al., Three-dimensional carbon nanotube/transition-metal oxide sponges as composite electrodes with enhanced electrochemical performance, ACS Appl. Nano. Mater 1 (2018) 2997–3005.

[41] D. Wang, K. Wang, L. Sun, H. Wu, J. Wang, Y. Zhao, et al., MnO2 nanoparticles anchored on carbon nanotubes with hybrid supercapacitor-battery behavior for ultrafast lithium storage, Carbon 139 (2018) 145–155, https://doi.org/10.1021/acsanm.8b00606.

[42] Y.X. Yin, S. Xin, Y.G. Guo, L.J. Wan, Lithium−Sulfur batteries: electrochemistry, materials, and prospects, Angew. Chem. 52 (2013) 13186–13200, https://doi.org/10.1002/anie.201304762.

[43] F.C. De Godoi, D.W. Wang, Q. Zeng, K.H. Wu, I.R. Gentle, Dependence of LiNO$_3$ decomposition on cathode binders in Li-S batteries, J. Power Sources 288 (aug.15) (2015) 13–19, https://doi.org/10.1016/j.jpowsour.2015.04.064.

[44] H. Wu, L. Wang, J. Bi, Y. Li, X. Pang, Z. Li, et al., Local concentration effect derived heterogeneous Li$_2$S$_2$/Li$_2$S depositing on dual-phase MWCNT/cellulose nanofiber/NiCo2S4 self-standing paper for high performance of lithium polysulfide batteries, ACS Appl. Mater. Interfaces 12 (13) (2020) 15228–15238, https://doi.org/10.1021/acsami.0c00618.

[45] L. Jia, J. Wang, Z. Chen, Y. Su, W. Zhao, D. Wang, et al., High areal capacity flexible sulfur cathode based on multi-functionalized super-aligned carbon nanotubes, Nano Res 2 (5) (2019) 1105–1113, https://doi.org/10.1007/s12274-019-2356-1.

[46] M. Xiang, H. Wu, H. Liu, J. Huang, Y. Zheng, L. Yang, et al., A flexible 3D multifunctional MgO-decorated carbon foam@ CNTs hybrid as self-supported cathode for high-performance lithium-sulfur batteries, Adv. Funct. Mater. 27 (37) (2017) 1702573, https://doi.org/10.1002/adfm.201702573.

[47] Q. Pang, X. Liang, C.Y. Kwok, J. Kulisch, L.F. Nazar, A comprehensive approach toward stable lithium−sulfur batteries with high volumetric energy density, Adv. Energy. Mater 7 (6) (2017) 1601630, https://doi.org/10.1002/aenm.201601630.

[48] Y. Zhang, K. Li, H. Li, Y. Peng, Y. Wang, J. Wang, et al., High sulfur loading lithium−sulfur batteries based on a upper current collector electrode with lithium-ion conductive polymers, J. Mater. Chem. A 5 (1) (2017) 97–101, https://doi.org/10.1039/C6TA08264E.

[49] M. Xiang, L. Yang, Y. Zheng, J. Huang, P. Jing, H. Wu, et al., A freestanding and flexible nitrogen-doped carbon foam/sulfur cathode composited with reduced graphene oxide for high sulfur loading lithium−sulfur batteries, J. Mater. Chem. A 5 (34) (2017) 18020–18028, https://doi.org/10.1039/C7TA04962E.

[50] H. Shi, S. Niu, W. Lv, G. Zhou, C. Zhang, Z. Sun, et al., Easy fabrication of flexible and multilayer nanocarbon-based cathodes with a high areal sulfur loading by electrostatic spraying for lithium-sulfur batteries, Carbon 138 (2018) 18–25, https://doi.org/10.1016/j.carbon.2018.05.077.

[51] J. Zhang, C. You, J. Wang, H. Xu, C. Zhu, S. Guo, et al., Confinement of sulfur species into heteroatom-doped, porous carbon container for high areal capacity cathode, Chem. Eng. J. 368 (2019) 340–349, https://doi.org/10.1016/j.cej.2019.02.171.

[52] Y. Han, X. Duan, Y. Li, L. Huang, D. Zhu, Y. Chen, Effects of sulfur loading on the corrosion behaviors of metal lithium anode in lithium−sulfur batteries, Mater. Res. Bull. 68 (2015) 160–165, https://doi.org/10.1016/j.materresbull.2015.03.042.

[53] M. Hagen, G. Feisthammel, P. Fanz, H.T. Grossmann, S. Dorfler, J. Tubke, et al., Sulfur cathodes with carbon current collector for Li-S cells, J. Electrochem. Soc. 160 (6) (2013) A996–A1002, https://doi.org/10.1149/2.149306jes.

[54] R. Ummethala, M. Fritzsche, T. Jaumann, J. Balach, S. Oswald, R. Nowak, et al., Lightweight, free-standing 3D interconnected carbon nanotube foam as a flexible sulfur host for high performance lithium-sulfur battery cathodes, Energy Storage Mater 10 (2018) 206–215, https://doi.org/10.1016/j.ensm.2017.04.004.

[55] J.H. Yun, J.H. Kim, D.K. Kim, H.W. Lee, Suppressing polysulfide dissolution via cohesive forces by interwoven carbon nanofibers for high-areal-capacity lithium−sulfur batteries, Nano Lett. 18 (1) (2017) 475–481, https://doi.org/10.1021/acs.nanolett.7b04425.